THE JOURNAL OF PHYSICAL CHEMISTRY B

Article

pubs.acs.org/JPCB

Photocontrol of Reversible Amyloid Formation with a Minimal-Design Peptide

Steven A. Waldauer,[‡] Shabir Hassan,[‡] Beatrice Paoli,[†] Paul M. Donaldson,[‡] Rolf Pfister,[‡] Peter Hamm,*[,‡] Amedeo Caflisch,*[,†] and Riccardo Pellarin*[,†,§]

[†]Department of Biochemistry, University of Zurich, Winterthurerstrasse 190, CH-8057 Zurich, Switzerland

[‡]Institute of Physical Chemistry, University of Zurich, Winterthurerstrasse 190, CH-8057 Zurich, Switzerland

[§]Department of Bioengineering and Therapeutic Sciences, University of California in San Francisco, 1700 Fourth Street, San Francisco, California 94158, United States

Supporting Information

ABSTRACT: Amyloid aggregates are highly ordered fibrillar assemblies of polypeptides involved in a number of neurodegenerative diseases. Very little is known on the pathways of self-assembly of peptides into the final amyloid fibrils, which is due in part to the difficulty of triggering the aggregation process in a controlled manner. Here we present the design and validation of a cross-linked hexapeptide that reversibly aggregates and dissociates under ultraviolet light irradiation control. First molecular dynamics simulations were carried out to identify, among hundreds of possible sequences, those with the highest propensity to form ordered (β-sheet) oligomers in the trans state of the azobenzene cross-linker, and at the same time with the highest solubility in the cis state. In the simulations, the peptides were observed to spontaneously form ordered oligomers with cross-β contacts when the cross-linker was in the trans state, whereas in the cis state they self-assemble into amorphous aggregates. For the most promising sequence emerging from the simulations (Ac-Cys-His-Gly-Gln-Cys-Lys-NH_2 cross-linked at the two cysteine residues), the photoisomerization of the azobenzene group was shown to induce reversible aggregation by time-resolved light scattering and fluorescence measurements. The amyloid-like fibrillar topology was confirmed by electron microscopy. Potential applications of minimally designed peptides with photoswitchable amyloidogenic propensity are briefly discussed.

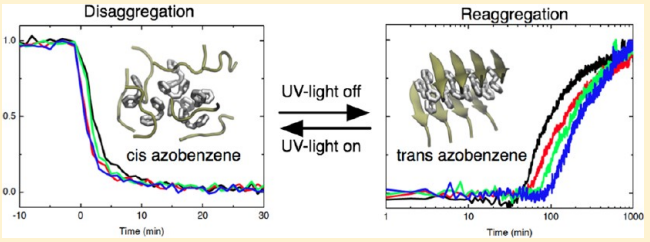

I. INTRODUCTION

Amyloidogenesis has been implicated as an important factor in a number of neurological and systemic diseases.[1] Amyloid fibrils, the products of amyloidogenesis, consist of ordered self-assemblies of polypeptides stabilized by intermolecular cross-β contacts (β-interactions). They form with a characteristic fibrillar morphology which often collect cellularly into larger structures such as plaques in Alzheimer's and Lewy bodies in Parkinson's diseases.[2,3] The cytotoxicity of amyloid aggregation has been linked to the presence of intermediates. For example, studies have shown that it may be the prefibrillar aggregates that cause cell death in Alzheimer's disease[4] and not the large mature fibrils found in the same tissues. In fact, the amyloid fibril formation is a multistep process that involves a nucleation phase, where initial oligomers assemble, and an elongation phase, during which protofibrillar intermediates are formed[5−8] and grow to mature fibrils by monomer docking and peptide structural rearrangement.[9,10]

To unravel the nature of amyloid aggregation, it is crucial to understand the pathways and the structural details of the earliest steps in self-assembly. Computer simulation of polypeptide self-aggregation has shed some light on the process of amyloidogenesis. Atomistic models have been employed to study the conformational space of amyloidogenic polypeptides in the monomeric state,[11,12] the very initial steps of amyloid formation,[13−19] and the structural stability of fibril models.[20−24] In particular, simulation studies of early oligomerization, involving a few peptides or polypeptide fragments, have provided important insight into the detailed molecular mechanism and sequence determinants in amyloid formation,[13,14,16,25−29] aggregation inhibition,[30−33] and nucleation.[19,34,35]

Experimentally, it is possible to measure early events of aggregation in vitro using stopped-flow or other mixing methods;[36] however, amyloid aggregation can be unpredictable and difficult to work with. Often, the onset of aggregation starts immediately following the initial preparation of a peptide solution, well before any measurement is possible. For other solutions, it can take between minutes and days for aggregation to start and can vary from preparation to preparation even with identical peptide sequences or different portions of the same sample.[37] Many groups have found solutions to these problems.

Received: May 31, 2012
Revised: June 21, 2012

dx.doi.org/10.1021/jp305311z | J. Phys. Chem. B XXXX, XXX, XXX−XXX

For example, by modifying amyloid peptide sequences through the introduction of a "host−guest switch", aggregation can be initiated reliably upon the addition of an enzyme or change in pH.[38] These modifications facilitate time-resolved experiments studying aggregation growth; however, many of the standard mixing experiments such as stopped-flow are still limited by the time resolution of the detector or by the dead-time of the instruments. One method that resolves these limitations is to use photocontrol as a trigger for aggregation, for example, by modifying the amyloid peptide with a photocleavable protective group that inhibits aggregation.[39] Others have demonstrated that the presence of a photosurfactant can inhibit amyloid aggregation depending on illumination.[40,41]

The photocontrol method used in this study was the incorporation of a photoswitchable molecule into a peptide, such that one photoisomer is more prone to amyloid fibril formation than the other. Among the various photoswitchable molecules, azobenzenes are extensively utilized in bottom-up design of biomaterials because of their efficient and reversible photoisomerization that leads to large changes in molecular geometry. Some studies have employed azobenzene-modified peptides as reversible aggregation units. In one study, a tripeptide fused with azobenzene forms fibrillar aggregates via β-sheet interactions.[42] In another work, two cyclic octapeptides are bridged by azobenzene whose isomerization state controls the conversion between intra- and intermolecularly assembled cylindrical structures.[43] It has been found that the aggregation propensity of a β-hairpin peptide with an azobenzene incorporated in the backbone changes depending on the conformation of the photoswitch.[44] Recently these studies have been extended to show that such a system can form amyloid-like structures when the azobenzene is in an extended conformation.[45]

The present work is motivated by the following question: what is the minimal possible design of a photoswitchable peptide whose amyloid association can be triggered and reversed in a controllable manner? We attempt to answer this question by employing a simulation-based approach, where we design an azobenzene cross-linked peptide whose equilibrium between the β-aggregation prone and soluble conformations is photocontrollable. Given the minimal length of the peptide, the design process was based on an almost exhaustive screening of peptide mutations, simulated and selected based on their self-aggregation behavior. Experimental assays performed on the selected sequence show that the synthesized photocontrollable peptide does form amyloid-like fibrils when the photoswitch is in an extended conformation and that the aggregates disassociate upon illumination such that the cross-linker is switched into a compact conformation. Moreover, this process of aggregation and disassociation can be repeated multiple times on the same sample.

II. MATERIALS AND METHODS

Simulation Protocols. All simulations were performed with the program CHARMM.[46] For the implicit solvent simulations, the peptides were modeled using the united hydrogen force field PARAM19 that explicitly accounts for heavy atoms and polar hydrogens bound to nitrogens or oxygens. The default truncation scheme for nonbonding interactions was set to 7.5 Å. Protonation states of titratable residues were set according to those found at pH 7.0. During the first sequence selection, an efficient mean field approximation based on the solvent accessible surface area (SASA) was used to describe the main effects of the aqueous solvent.[47] Formal charges were neutralized, and electrostatic screening was emulated by a distance dependent dielectric constant. For the second sequence selection, a more accurate generalized Born implicit solvent (FACTS) was used with non-neutralized formal charges.[48] Nonpolar solvation was approximated by a term proportional to surface area with a multiplicative surface-tension-like parameter of 7.5 kcal/(mol·Å^{-2}). SHAKE was used to fix the covalent bonds involving polar hydrogens.[49] All implicit solvent simulations were carried out with periodic boundary conditions at a fixed peptide concentration of 5.3 mM (corresponding to a box size of 98 Å for the trimer and 135 Å for the octamer simulations), using Langevin integration of motion equations with a time step of 2 fs, low friction constant (0.1 ps^{-1}), and at a constant temperature of 330 and 310 K for the SASA and FACTS simulations, respectively. Simulations were performed with either three or eight replicas of the same peptide sequence with all linkers either in the trans or cis conformation. The peptides were initially monodispersed and the configurations were individually equilibrated, to avoid biasing effects on the aggregation process. The aggregation simulations are sub-microsecond equilibrium simulations of the spontaneous oligomerization. A 1.0 μs run with implicit solvent takes less than 1 week on a single AMD Opteron 252 CPU at 2.6 GHz.

The explicit water simulations were carried out using the CHARMM PARAM22 all-atom protein force field and the TIP3P model of water. An octahedral box of 50 Å per side was used; it contained 2613 water molecules in addition to 12 chloride and 4 sodium ions. Periodic boundary conditions were applied, together with the particle-mesh Ewald, which was used for the long-range electrostatic interactions. The van der Waals interactions were truncated at a cutoff of 12 Å, and a switch function was applied starting at 10 Å. The trajectories were produced at 300 K, kept constant using a Nosé−Hoover thermostat, and a pressure of 1 atm using a Langevin piston, with an integration time step of 2 fs. An equilibration of 0.5 ns was performed before the production runs which consisted of 200 ns (two runs) and 50 ns.

Simulation Analysis. Since the simulations were run under different conditions (i.e., cis and trans configurations, different implicit solvents), there was not a single observable that was optimally sensitive to rank the sequences for all the selection steps. Therefore, to evaluate the aggregation propensity of the simulated peptide sequences, a number of observables were introduced, as discussed below, and the sequence ranks were made by choosing the observable with the highest sensitivity upon sequence change. For instance, the first sequence selection, based on SASA implicit solvent simulations, was performed by ranking the sequences using the order parameter, whereas in the second selection we used the number of backbone hydrogen bonds and radius of gyration for the trans and cis systems, respectively.

Order Parameters. Nematic and polar order parameters P_2 and P_1, originally introduced to describe the molecular arrangement of liquid crystals,[50,51] are useful quantities to monitor the structural transition within peptide oligomers.[16,52] The order parameter P_2 measures the amount of β-structure of the system by determining the fraction of aligned molecular components, here represented by N molecular unit vectors $\hat{\mathbf{z}}_i$ that join the C_α atom of residue i to the C_α atom of residue i + 2. P_2 is defined as

dx.doi.org/10.1021/jp305311z | J. Phys. Chem. B XXXX, XXX, XXX−XXX

$$P_2 = \frac{1}{N}\sum_{i=1}^{N}\frac{3}{2}(\hat{\mathbf{z}}_i\cdot\hat{\mathbf{d}})^2 - \frac{1}{2}$$

where the unit vector $\hat{\mathbf{d}}$ defines the predominant direction of all molecular unit vectors, and is obtained as the eigenvector of the ordering matrix that corresponds to the largest positive eigenvalue. The values of P_2 range from 0 to 1, which respectively correspond to complete disorder and complete order. Complete order is achieved when all the unit vectors are parallel or antiparallel, while the disorder is obtained when none of the unit vectors are parallel to any of the others. Since the P_2 parameter distribution of a trimer that reversibly oligomerizes into ordered structures is typically bivariate, with one peak close to 1 and a broad peak at 0.5, to assess the order of a full equilibrium trajectory, we found it convenient to define the order−disorder ratio rP_2, which is the frequency that the order parameter is lower than a cutoff value $P_2^* = 0.65$ (disorder) divided by the frequency that it is higher than P_2^* (order). The cutoff value was determined to maximize the sensitivity of rP_2 (see ref 30).

The polar order parameter P_1 accounts for the number of molecular vectors $\hat{\mathbf{z}}_i$ pointing in the same direction, and discriminates between parallel and antiparallel/mixed ordered aggregates, for which P_1 has a value of 1 and 0, respectively. It is defined as

$$P_1 = \frac{1}{N}\sum_{i=1}^{N}\hat{\mathbf{z}}_i\cdot\hat{\mathbf{d}}$$

Hydrogen Bonds. The number of intermolecular and intramolecular backbone hydrogen bonds was used to quantify the propensity of the peptides to form cross-β interactions. The criteria for hydrogen bonds are a H−O distance shorter than 2.5 Å and a NH−O angle larger than 130°.

Radius of Gyration. The radius of gyration R_g was used to quantify the compactness of the oligomers. It is evaluated as the square root of the mean squared deviation of the Cα atom positions from the geometric center of the oligomer $R_g^2 = (1/N)\sum_{i=1}^{N}(r_i - r_{mean})^2$. A high value (>22 Å) corresponds to a dissociated trimer, while a low value (<10 Å) is a compact trimer. rR_g is the ratio between the number of trajectory frames where R_g is higher and lower than the threshold value of 14 Å, empirically set according to R_g frequency distribution evaluated along the simulations (see Figure S3, Supporting Information).

Parametrization of the Cross-Linker. The atom types that comprised the cross-linker were derived from the PARAM19 and PARAM22 force fields for the implicit and explicit solvent simulations, respectively (see ref 53 for more details). The cis and trans isomerization states of the C—N═N—C bond are enforced by a dihedral potential with a single minimum at 0 and 180°, respectively.

Construction of the Cross-Linked Peptide Model. Initial models of the cross-linked peptide with the azobenzene in the trans or cis configuration were built from the extended configuration of the peptide. The two cysteine S_γ atoms were attached to each half of the cross-linker, which was split at the N═N bond. Initially the modified side chains were arbitrarily oriented, violating the N═N bond length. A dihedral potential with a minimum at the angle corresponding to the trans (or cis) configuration was then applied at the C—N═N—C bond. The model was then minimized to get rid of clashes and violated bonds, restoring the integrity of the cross-linker.

Peptide Synthesis and Cross-Linking. The azobenzene cross-linker was synthesized and fused to the peptide according to the procedure detailed in ref 54. The His.Gln peptide, with sequence Ac-Cys-His-Gly-Gln-Cys-Lys-NH_2, was purchased from GL Biochem Ltd. (Shanghai). The product was then further purified by high pressure liquid chromatography. Any residual TFA was removed using an ion exchange column (Varian BOND ELUT SAX, Agilent Life Sciences). The final product was then resuspended in buffer and filtered through a 0.22 μm filter before use in aggregation experiments.

Fibril Formation. Stock solutions of cross-linked peptides were prepared in 10 mM phosphate buffer at various pH values, a final concentration of about 0.3 mM, and a volume of 3 mL in a quartz 10 mm path length cuvette. The solutions were stirred continuously by a small magnetic stir bar, which was periodically lifted once per minute for about 2−3 s to inhibit aggregation on the surfaces of the cuvette. Aggregation became visible (the solution would appear cloudy) within hours to days after the initial suspension of the peptides.

Scattering Studies. Scattering measurements were taken using a home-built apparatus described briefly as follows: a red LED provided the source of the scattered light and a phototransistor, mounted at 90° from the source, was used to measure the scattered light. The light source was modulated at about 3 kHz, and any scattered light produced by particles such as fibrils was collected on the detector. The signal was then amplified and run through a high-pass filter, rectified, and read by an AD converter. A microprocessor controlled both the apparatus and recorded measurements. The entire apparatus was compact enough that it could be placed on top of a magnetic stir plate such that the solution was stirred continuously and any aggregates could not settle to the bottom of the cuvette. The apparatus also included a small, mechanically controlled magnet that could be lowered adjacent to the cuvette such that the oscillating stir bar was raised to the upper half of the solution and then dropped, controlled automatically by the apparatus microprocessor. This motion took about 2 or 3 s, was set to occur periodically every minute, and was important to inhibit the production of aggregation on the surfaces of the cuvette. A 365 nm wavelength LED was used to switch the conformation of the azobenzene photoswitch from trans to cis. Since the UV light source was not modulated, it did not add to the scattering signal.

TEM Imaging. Peptide solutions were prepared in 10 mM sodium phosphate buffer at varying pH with a final concentration of about 0.3 mM and allowed to aggregate for at least 24 h. Samples were taken from the aggregated peptide solutions (6 μL) and applied to previously glow discharged, carbon-coated 300 mesh copper grids, for 1 min. The excess solution was immediately blotted dry with filter paper, and the grids were then stained for 2 min with 2% (w/v) uranyl acetate in water. Microscopy was performed with a Philips CM100 transmission electron microscope operating at an accelerating voltage of 80 kV. High-resolution TEM images were captured with a fitted 4k × 3k pixel 12-bit Gatan digital camera. TEM images comparing trans and cis conformations were taken from the same solutions previously used in scattering measurements to observe photoinitiated disassociation and reaggregation.

Fluorescence Measurements. Solutions were prepared according to Nilsson et al. (ref 55), and are briefly described here: A stock solution of PTAA-Li was prepared at a concentration of 1 mg/mL in deionized water. A 10 μL portion of this solution was mixed with 15 μL of the peptide

dx.doi.org/10.1021/jp305311z | J. Phys. Chem. B XXXX, XXX, XXX−XXX

solution and diluted to a final volume of 2 mL in 20 mM pH 7 phosphate buffer. The solution was incubated at room temperature for 5 min. Emission and excitation spectra were recorded with a HORIBA Jobin Yvon, Fluorolog 3 fluorometer.

III. SIMULATION RESULTS

Initial Sequence Design. One basic premise behind our photoswitchable peptide sequence design is that the β-aggregation prone conformation corresponds to a fully extended configuration of the peptide. In this conformation, we assume that the backbone amide hydrogens and carbonyls are solvent exposed and susceptible to involvement in intermolecular hydrogen bonds. This premise, along with the characteristics of the azobenzene-derived cross-linker, described by the Woolley group,[54] introduce much of the primary restraints for a minimal amyloid peptide design. The cross-linker is anchored to the peptide at both ends to cysteine residues by thiol chemistry, and has two photoisomers: a compact cis state and an extended thermally stable lower-energy trans state. Therefore, the end-to-end distance of the cross-linker in the trans state dictates the size of the peptide, which we found to be about five residues, named here X_1−X_5 counting from the N-terminus. In order to anchor the cross-linker, X_1 and X_5 must be cysteine residues, leaving $X_2X_3X_4$ free to be varied systematically. Isomerization can be driven in both directions: from trans to cis by illuminating with 365 nm light, or in the other direction by 430 nm light. In our design, the trans conformation of the cross-linker induces an aggregation prone conformation of the peptide. Preliminary simulations and computer modeling (not shown) revealed that the cross-linked pentapeptide tolerates isomerization of the photoswitch by altering the structure of the peptide backbone. When the linker is in the cis state, the peptide backbone rearranges into a collapsed configuration, which is an ideal β-aggregation protected conformation, since the backbone amide hydrogens and carbonyls are sequestered by intramolecular hydrogen bonds, reducing their ability to form ordered cross-β interactions. The peptide is capped by uncharged acetyl and N-methylamide groups at the N- and C-terminus, respectively.

Selection of the Sequences. We chose a simulation-based strategy to design a minimal-length sequence for the cross-linked peptide, which we then validated by further simulations and experiments. The design had two fundamental requirements: first, the sequence must have the highest β-aggregation propensity when the cross-linker is in the trans conformation, and second, it must have the highest solubility in the cis conformation. The combination of these two opposing requirements determined the peptide sequence with the most distinct transition between the amyloid-prone and the soluble state. We organized the sequence design process (Figure 1) by progressively increasing the complexity of the system from implicit solvent simulations of trimeric systems to the final experimental validation of the selected sequence (see Table 1). We estimated the β-aggregation propensity of a given sequence using the order parameters P_1, P_2, and rP_2 (see Materials and Methods), which account for the amount of parallel structure and molecular order in the oligomers, and the number of intramolecular backbone hydrogen bonds over the produced simulation trajectories.

Effect of Alanine and Glycine at Position X_3. Computer modeling of the trans state cross-linked peptide, with X_2 and X_4 set to alanines and X_3 spanning a number of different residues (not shown), revealed that position X_3 must be occupied by a small residue, either glycine or alanine. In fact, when the peptide backbone is in a β-conformation, the side chain at position X_3 points in the same direction as the X_1 and X_5 cysteine side chains with respect to the plane defined by the β-sheet, and clashes against the linker. Implicit solvent aggregation simulations of trimeric CAGAC and CAAAC sequences with the cross-linker in the trans state revealed that an alanine side chain at position X_3 is sufficiently large to hinder ordered β-aggregation, as revealed by the decreased nematic order parameter ratio rP_2, the decreased number of intermolecular hydrogen bonds, and the increased radius of gyration (see Table 2). We therefore decided to proceed by setting position X_3 to glycine on all subsequent sequence screenings.

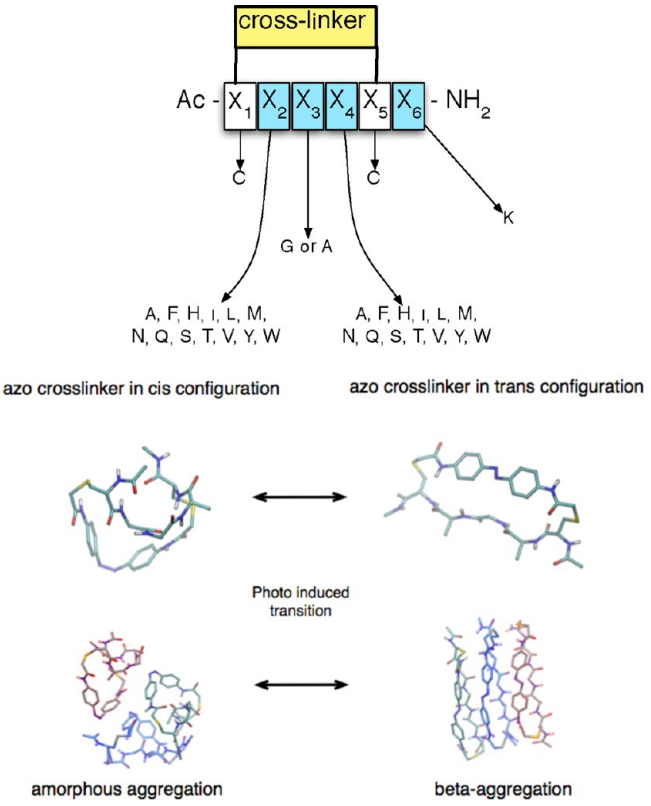

Figure 1. Photoswitchable aggregation. Top: Diagram showing the basic structure of the minimal peptide sequence design for photoswitchable aggregation and a summary of all explored variants. Bottom: The cross-linked peptide undergoes isomerization between the cis and trans conformations upon UV illumination (left) and UV-light absence (right). The backbone of monomer in the cis conformation is collapsed and unable to form cross-β interactions. In the trans conformation, the backbone is extended and prone to form amyloid-like interactions.

Positions X_2 and X_4, First Selection Round. Using implicit solvent simulations, we filtered out all sequences that were not able to oligomerize into ordered β-structures with the cross-linker in the trans configuration. At positions X_2 and X_4, we considered all possible residue combinations, excluding those with charged side chains (to avoid electrostatic repulsion), proline and glycine (which are β-breaker residues), and cysteine (to avoid incorrect cross-linking to the peptide). This left 169 possible sequences, which we have labeled with the compact symbol $X_2.X_4$ (shorthand for the full sequence Cys-X_2-Gly-X_4-Cys), each of which were modeled in the trans configuration and used in trimeric aggregation simulations

dx.doi.org/10.1021/jp305311z | J. Phys. Chem. B XXXX, XXX, XXX−XXX

Table 1. Design Procedures[a]

design stage	sequences	number of sequences	approach	solvent model	system size	linker state
selection	CA[A,G]AC	2	simulation	SASA	trimer	T
selection	CXGXC	169	simulation	SASA	trimer	T
selection	CXGXCK	26	simulation	FACTS	trimer	T,C
selection	selected sequences	4	simulation	FACTS	octamer	T,C
validation	selected sequences	1	simulation	TIP3P	octamer	T
validation	selected sequences	1	experiments		multimer	T,C

[a]The design pipeline was organized as a progressive selection of sequences based on the results of molecular dynamics simulation with increasingly accurate solvent models: solvent accessible surface area implicit solvent (SASA),[47] fast analytical continuum treatment of solvation (FACTS),[48] and explicit TIP3P water molecules.[76]

Table 2. Effect of Glycine and Alanine at Position X_3[a]

sequence	time (ns)	rP_2	R_g	InterHB
CAGAC	420	0.62	7.89	1.75
CAAAC	420	0.06	9.09	0.40

[a]Nematic order parameter ratio (rP_2), radius of gyration (R_g), and intermolecular backbone hydrogen bonds (InterHB) calculated on trimer aggregation trajectory of two variants that have either alanine or glycine at position X_3.

using a SASA implicit solvent run for about 0.5 μs (see Materials and Methods).

During the simulations, the peptides sampled different oligomerization states, including monomers, dimers, and trimers, with different β-interaction arrangements (parallel, antiparallel, and mixed cross-β interactions). We ranked the equilibrium trajectories according to the average order parameter ratio rP_2 (Table S1, Supporting Information). Note that the number of intermolecular backbone hydrogen bonds correlates with rP_2 and that no intramolecular hydrogen bonds were formed due to the extended conformation of the peptides.

Positions X_2 and X_4, Second Selection Round. The 26 best ranked sequences of the first selection round were used to start trimer aggregation simulations using the FACTS[48] implicit solvent model (see Materials and Methods), which is more accurate but less efficient than SASA. Taking into account the limitations of F-moc synthesis for any peptides that might be synthesized for experiments, the sequences were modified by appending a lysine at the C-terminus of the peptide in order to increase the yield and solubility. All 26 sequences were simulated with the cross-linker in the cis and trans conformations, for a total of 52 simulations. Compared to SASA, FACTS implicit solvent is closer to an aqueous environment because of higher effective dielectric screening. This resulted in less compact and more disordered oligomers, and the rP_2 parameter became too noisy to measure appreciable differences between the sequences. For this reason, the trans simulations were instead ranked according to increasing average number of intermolecular hydrogen bonds, which in this case is more suitable and sensitive to structural changes (Tables 3 and S2, Supporting Information). The cis simulations were ranked according to increasing values of the radius of gyration ratio rR_g, in order to favor sequences that are more soluble (Tables 3 and S3, Supporting Information). The total score used to rank each sequence was determined by summing the individual ranks of the cis and trans simulations. Hence, lowest scored (i.e., highly ranked) sequences corresponded to the variants with the most desired properties (i.e., being β-aggregation prone in the trans configuration and soluble in the cis configuration).

Table 3. Final Ranks of the Peptide Sequences Taken from the Second Round of Aggregation Simulations[a]

X_2.X_4	cis	trans	score
His.Ala	**6**	**4**	**10**
His.Gln	**7**	**8**	**15**
Phe.Ala	**11**	**6**	**17**
His.Met	**9**	**11**	**20**
His.Leu	12	9	21
Tyr.Tyr	19	2	21
His.Phe	16	7	23
His.Asn	8	16	24
His.His	14	10	24
Phe.Tyr	21	3	24
Met.Ala	4	21	25
His.Trp	26	1	27
Met.Trp	10	17	27
Ser.Ala	1	26	27
Thr.Met	3	24	27
Val.Thr	2	25	27
Val.Asn	5	23	28
Leu.Phe	18	12	30
Phe.Trp	25	5	30
Phe.His	17	15	32
Phe.Met	15	18	33
Leu.His	13	22	35
Tyr.Phe	22	14	36
Phe.Phe	24	13	37
Trp.Met	20	19	39
Trp.Val	23	20	43

[a]The score is calculated as the sum of the rank numbers obtained from the cis and trans simulations (Tables S2 and S3, Supporting Information). A low score (i.e., high rank) corresponds to sequences that are highly prone to form β interaction in the trans state and at the same time display high solubility in the cis state. The highest ranking sequences are highlighted in boldface in the table, and are chosen to start octameric aggregation simulations. The full sequence of the simulated cross-linked peptide is Ac-Cys-X_2-Gly-X_4-Cys-Lys-NH_2.

Octamer Simulations. We selected the four highest ranking sequences, X_2.X_4 = His.Ala, His.Gln, Phe.Ala, His.Met (Table 3), for octamer aggregation simulations, with all the cross-linkers in either trans or cis configurations. Visual inspection of the trajectories revealed that in the trans configuration the initially monodispersed peptides spontaneously nucleated into β-sheet containing aggregates with transiently different registers and arrangements (Figures 2 and 3), as reflected by the fluctuations in the number of intermolecular backbone hydrogen bonds (see Figure S2, Supporting Information). Structural analysis of the four aggregation simulations (Figure 2f) showed that among all

dx.doi.org/10.1021/jp305311z | J. Phys. Chem. B XXXX, XXX, XXX–XXX

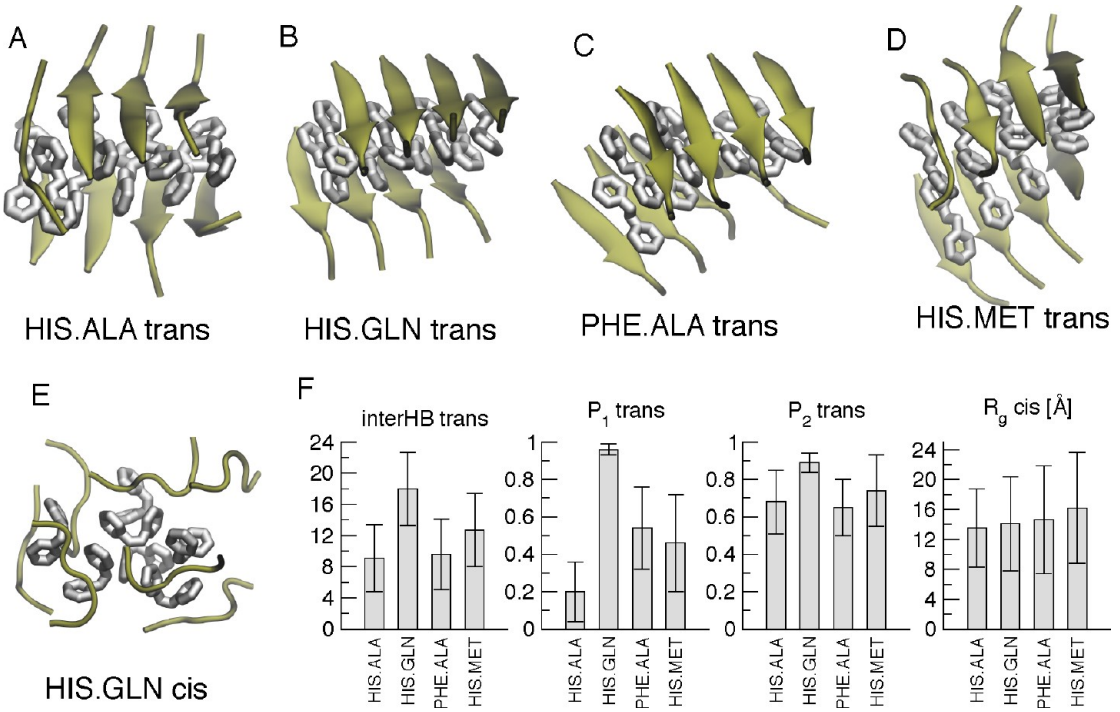

Figure 2. Simulation snapshots. (a–d) Octamer conformations extracted from implicit solvent simulation trajectories of aggregation with the cross-linker in the trans conformation. For clarity, the side chains that connect the azobenzene to the peptide backbone are not represented. The snapshots correspond to the conformations with the highest amount of backbone hydrogen bonds, explored by the octamer. (e) Aggregation trajectory snapshot when the cross-linker is in the cis conformation, showing a micellar-like morphology. (f) From left to right: time average of the number of intermolecular backbone hydrogen bonds, polar order parameter P_1, nematic order parameter P_2 for aggregation simulations in the trans state, and average radius of gyration R_g for the simulations in the cis state. Error bars indicate the standard deviation. The averages are calculated omitting the first 100 ns of simulation.

sequences His.Gln had the highest amount of intermolecular backbone hydrogen bonds, as well as the highest molecular order and parallel aggregation content, as shown by the P_2 and P_1 order parameters. Although having different stabilities, the four sequences mainly nucleated into two β-sheet ordered structures, with the azobenzene acting as a hydrophobic surface buried in the interior.

The nucleation of the His.Gln ordered aggregate and the formation of the cross-β interactions occurred in a disordered micellar oligomer (Figure 3). After about 8 ns, the first dimer associated through intermolecular contacts between the azobenzene moieties. In the subsequent 100 ns, the other six monomers attached to the dimer by establishing hydrophobic contacts through the cross-linkers. At this stage, the oligomer displayed the properties of a disordered micelle, with the hydrophobic azobenzene moieties buried inside and the hydrophilic histidine, glutamine, and lysine side chains pointing outward. On average, the micellar octamer had a total of seven backbone intermolecular hydrogen bonds (less than one per monomer), and transiently formed a β-sheet structure. In the following 50 ns, ordered cross-β interactions propagated quickly, as shown by the increasing number of intermolecular hydrogen bonds, to an average of 17.

Visual inspection of the nucleation process revealed that the formation of the amyloid oligomer is a two-step structural rearrangement. When the first four-stranded β-sheet is formed, the oligomer is half-ordered and half-disordered. The two halves are in contact through the eight azobenzenes, where the four belonging to peptides integral to the β-sheet are stably arranged in a stack, and the remaining azobenzenes are unspecifically attached. The ordered tetramer part induces β-sheet formation on the disordered part within about 30 ns. The resulting structure, two parallel β-sheets assembled through azobenzene interactions, is very stable and does not change throughout the following 900 ns.

When the cross-linker is in the cis conformation, the peptides assemble into disordered aggregates with few intermolecular and intramolecular hydrogen bonds (Figures 2e, 3b, and S1, Supporting Information) and with low molecular order (P_2 ~0.3). A comparison of the radius of gyration frequency distributions between the cis and trans His.Gln aggregates shows that in the former state, due to the weaker interactions between the peptides, the oligomer is less compact (Figure 3c). In the cis state of the cross-linker, the average radius of gyration R_g is independent of the simulated sequence (Figure 2f), and the aggregates appear as spherical micelles with the azobenzene buried inside (see Figure 2e), similar to the on-pathway oligomers initially formed during trans-peptide aggregation.

Explicit Water Simulations. The results of the octamer aggregation simulations above showed that the His.Gln peptide sequence is more prone to form stable and ordered oligomers. We decided to proceed with this sequence and validate the design with further computer simulations and experimental assays.

To assess the structural stability of the ordered aggregates formed in an implicit solvent, we started three explicit solvent simulations (Figure 5a) using the octamer conformation with the highest number of backbone hydrogen bonds explored during the previous trans aggregation simulations. In two of the trajectories, the parallel arrangement of the peptides and the cross-β interactions were conserved over the entire duration of the simulation. The Cα-rmsd value, with respect to the starting

dx.doi.org/10.1021/jp305311z | J. Phys. Chem. B XXXX, XXX, XXX–XXX

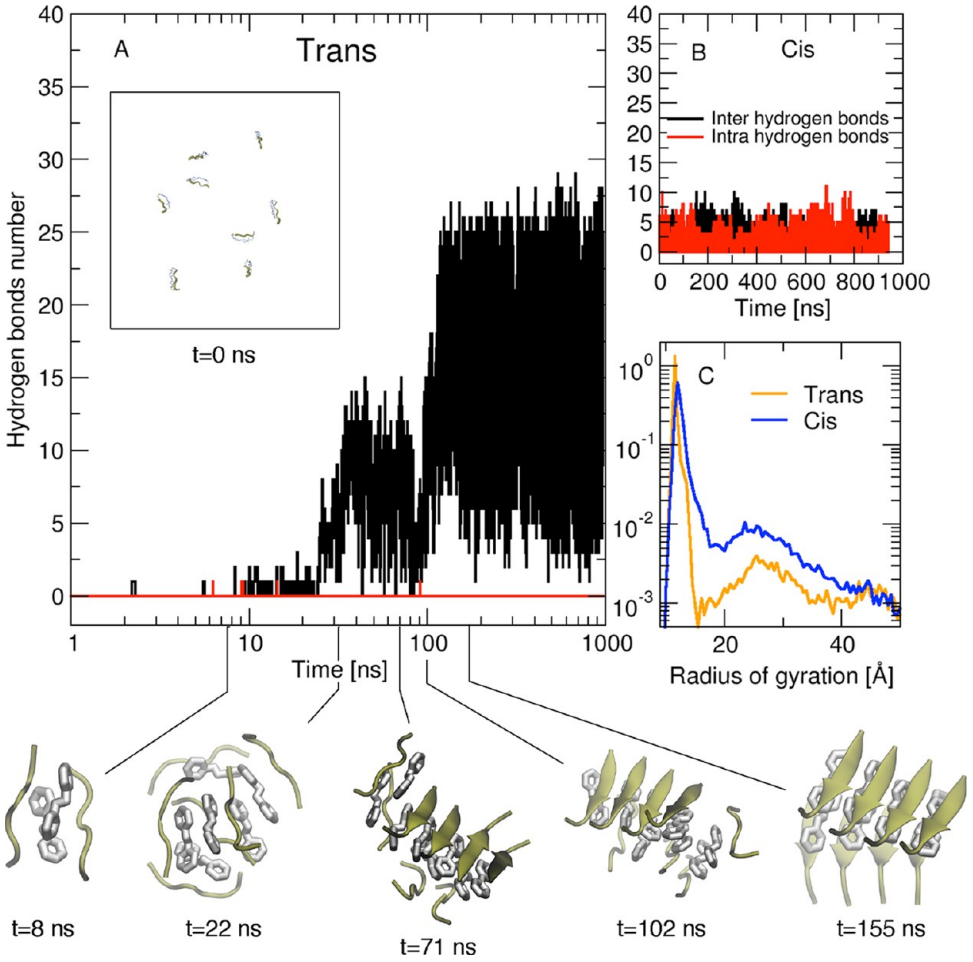

Figure 3. Octamer trajectory analysis. Number of intermolecular (black line) and intramolecular (red line) hydrogen bonds for the octamer simulations of the His.Gln peptide when the cross-linker is in trans configuration (a) and cis (b) configuration. The snapshots depict the aggregation process at selected times when the cross-linker is in the trans state. (c) Comparison between radius of gyration frequency histograms of the trans and cis simulations.

structure, is below 3 Å, and the oligomer has an average of about 17 intermolecular backbone hydrogen bonds, in agreement with the implicit solvent average value (see Figure 4a). Although in explicit solvent the oligomer did not substantially change the double β-sheet morphology formed in implicit solvent, it transiently explored two distinct arrangements of the azobenzene packing, showing that the ordered oligomer dynamically exchanges between alternate arrangements of the two β-sheets (Figure 4b and c). In one arrangement, each azobenzene fully interacts with a single corresponding facing linker (Figure 4b), whereas in the other arrangement it interacts with linkers belonging to two facing neighboring peptides (Figure 4c). Furthermore, visual inspection of the simulations revealed that the amide groups of the cross-linker are transiently involved in inter- and intra-β-sheet hydrogen bonds that contribute to the stability of the ordered oligomer (Figure 4e and f).

In the remaining simulation (simulation 2 in Figure 4a), after about 1 ns, two monomers at one edge of the oligomer separated from the β-sheets by breaking all backbone hydrogen bonds. The two monomers remained attached to the oligomer through nonpolar azobenzene interactions, and after 40 ns, one of the monomers dissociated, as revealed by the increase of Cα-rmsd. Besides the two disordered peptides, the remaining ordered hexamer, comprised of a double three-stranded β-sheet, basically conserved the same configuration as that in the original oligomer until the simulation was halted after about 50 ns (see orange time series in 4a).

IV. EXPERIMENTAL RESULTS

Aggregation Experiments. To test the aggregation properties of the photoswitchable peptide, we synthesized and cross-linked the His.Gln sequence. We measured the aggregation kinetics, assessed the photoinduced reversibility of the association, and determined the structural nature of the aggregation using three different series of experiments: static light scattering, fluorescence, and transmission electron microscopy (TEM). Static light scattering measurements were used to monitor the aggregation level of the peptides in the sample without giving information on the morphology of the aggregation itself. To determine the presence of amyloid structure and the fibrillar nature of the aggregated samples, we performed fluorescence binding assays using a new class of dyes and produced TEM images of the aggregants.

Scattering Experiments. We performed time-resolved light scattering experiments, measuring the level of aggregation on the His.Gln peptide under the presence and absence of UV light. The time-series of the scattered light intensity clearly confirmed the reversible association properties of the cross-linked peptide (Figure 5). In fact, the samples aggregated in the

dx.doi.org/10.1021/jp305311z | J. Phys. Chem. B XXXX, XXX, XXX–XXX

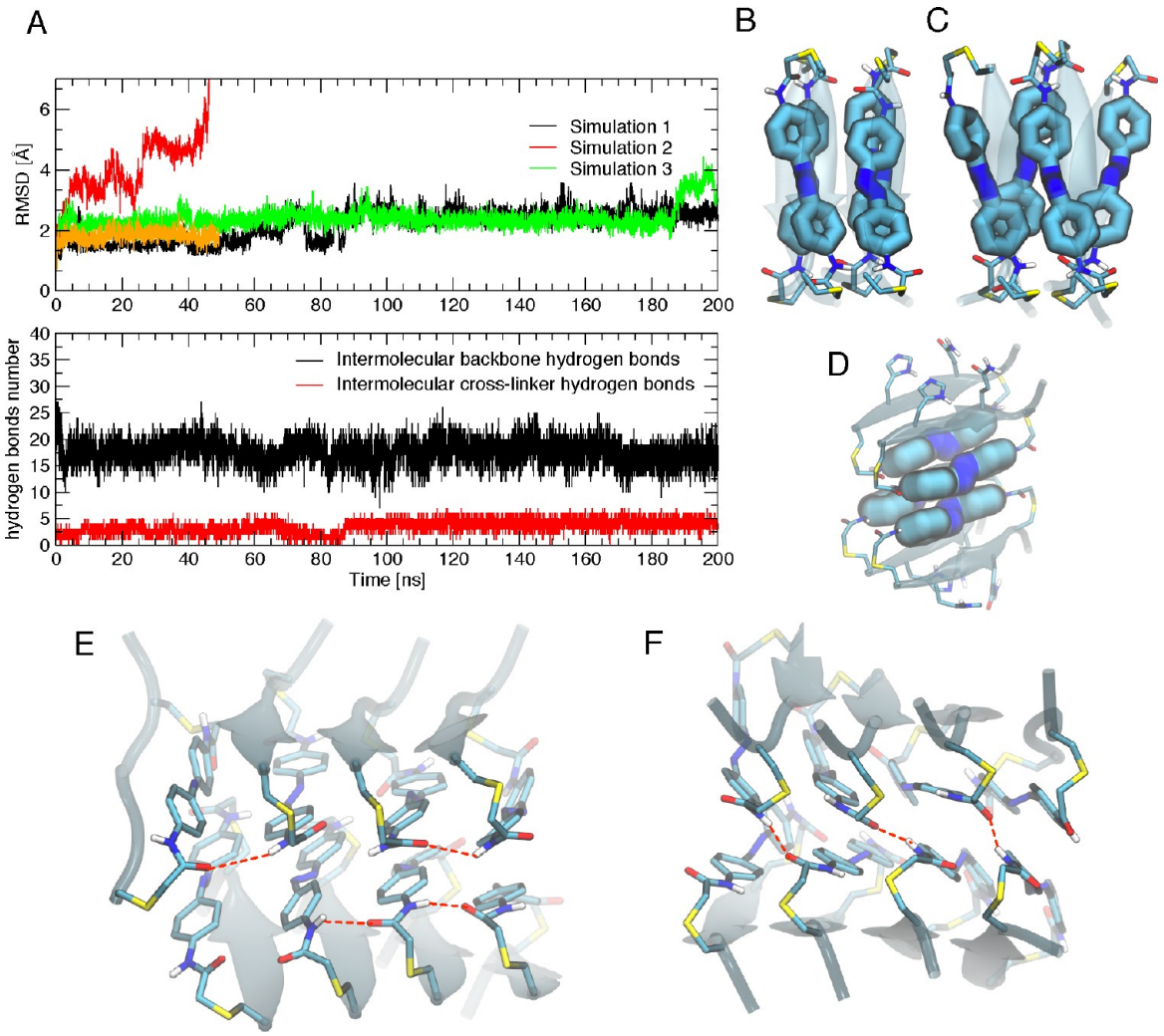

Figure 4. Structure of the amyloid oligomer. Structural analysis of the explicit solvent simulation trajectories of the ordered oligomer. The His.Gln peptide with the cross-linker in the trans conformation. (a) Top: C_α-rmsd time series with respect to the starting structure for three simulations. In one of the simulations, two peptides disaggregate from the oligomer, resulting in an increase of the octamer rmsd (red line), whereas the remaining six peptides are structurally stable as indicated by the rmsd calculated on the aggregated peptides (orange line). Bottom: backbone and cross-linker amide intermolecular hydrogen bonds calculated for simulation 1. The azobenzenes are arranged in two possible configurations (b, c) and packed inside the oligomer to form aromatic stacking interactions (d). The oligomer is stabilized by intra β-sheet (e) and inter β-sheet hydrogen bonds between the cross-linkers (f), represented by the red dashed lines.

absence of UV illumination and disassociated when exposed to UV light, much as predicted for the trans and cis conformation of the cross-linker. In a typical scattering experiment, a freshly prepared solution was placed in the light scattering instrument and monitored immediately with measurements taken every minute. The sample would begin to aggregate and light scattering was allowed to reach a steady maximum. The solution would then be illuminated under 365 nm UV light to induce disassociation until the scattering intensity reached a stable minimum. This sequence could then be repeated any number of times. A full aggregation trajectory, comprising the initial aggregation phase immediately after the peptide solution was produced, and a series of UV illuminations followed by UV-absent time intervals were typically run reproducibly over days to weeks.

Aggregation was found to have a strong pH dependence, with no sample prepared at a pH less than 5 showing aggregation even after more than 2 weeks of observation. Moreover, of the peptide solutions that did show aggregation, only those with pH 10 and lower showed signs of photo-induced disassociation with the largest change in scattering at pH 7. Interestingly, it was possible to observe association and disassociation for the pH 7 solutions by eye, in that the initial aggregated solution appeared cloudy and became clearer and darker, resembling the color of free azobenzene in solution following illumination with UV light (Figure S4, Supporting Information).

Upon initial suspension, aggregation showed a lag phase ranging from hours to days before an increase in scattering intensity could be detected. The aggregation process eventually reached equilibrium, indicated by a sustained maximum scattering. This lag phase is similar to that found in the non-photo-triggered studies mentioned in the Introduction, and in the same way, the lag time could vary from batch to batch. Light scattering disassociation curves, normalized and aligned such that time zero was when the UV light was first turned on, shown in Figure 5b, lie almost directly on top of each other, demonstrating that the disassociation kinetics are highly

dx.doi.org/10.1021/jp305311z | J. Phys. Chem. B XXXX, XXX, XXX–XXX

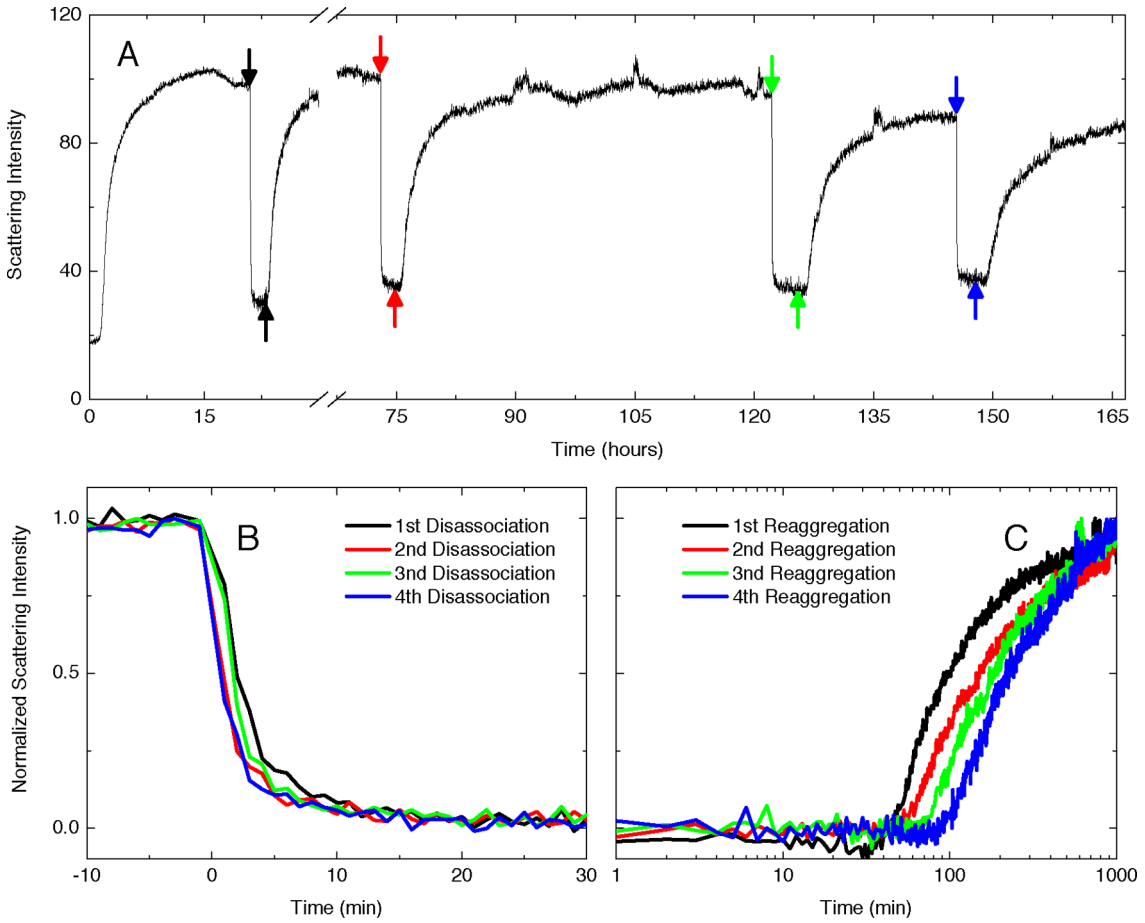

Figure 5. Light scattering. Light scattering was measured over 165 h continuously for a newly suspended solution of His.Gln peptide. (a) A full scattering trajectory showing the initial lag-phase, aggregation, and stable scattering maximum by 15 h and then four sequential photocontrolled disassociation and aggregation events. Downward arrows point to when UV illumination was initiated, and upward arrows point to when illumination was stopped. (b) Overlay of the four normalized disassociation events. Each colored curve is taken from the trajectory shown in part a and aligned such that each corresponding colored downward arrow is set to $t = 0$ min. (c) Overlay of the four normalized aggregation events, where $t = 0$ min corresponds to when UV illumination is removed and shown in part a by corresponding colored downward arrows.

repeatable. Reaggregation curves were also collected in the same manner, normalized and aligned such that time zero was when the UV light was turned off, shown in Figure 5c. The reaggregation kinetics show a lag phase, much like those of other aggregation experiments, with the delayed onset of measurable aggregation ranging from about 35 to 100 min after halting UV illumination, hence more predictable and reproducible than the initial aggregation. Also, the scattering baseline for the lag-phase of the initial aggregation is lower than the corresponding baselines for all of the photocontrolled disassociation. This could be explained by the emergence of micrometer-scale clumps of aggregates, large enough that the UV light source is not of sufficient intensity to convert 100% of the peptide photoswitches to the cis conformation and to disassociate the entire aggregate. Therefore, in the initially monodispersed sample, there were no scattering oligomers, whereas, at the end of each light-induced disassociation, aggregates were possibly present due to residual trans photoswitches, as evident from TEM micrographs (see below and Figure 7b). A small residual population of aggregation may also explain the smaller range of lag-times in the reaggregation kinetics in comparison with the initial aggregation. Photo-induced disassociation and reaggregation could typically be cycled multiple times over the course of weeks as long as the sample was kept sealed and stirred constantly.

Fluorescence. A typical test for assessing the presence of amyloid aggregates is by introducing Thioflavin T (ThT),[56] which changes in fluorescence upon binding with amyloid or amyloid-like fibrils. Specifically, an increase in emission intensity and a redshift of about 100 nm for the emission maximum is typically observed. Unfortunately, the emission and absorption spectra of ThT largely overlap with the absorbance spectra of the azobenzene derived photolinker, due to the structural similarity of the cross-linker and the ThT molecule. For similar reasons, absorbance measurements on Congo Red (another frequently used amyloid indicator) were also not attempted. Instead, we chose a new class of fluorescent dyes: luminescent conjugated polyelectrolyte probes (LCPs), which were specifically developed as markers for amyloid fibrils.[55,57] These dyes bind noncovalently with fibrils and have spectra that do not overlap with that of the photolinker. The LCP used in these experiments, polythiophene acetic acid (PTAA), has a fluorescence excitation maximum at about 400 nm and can still be excited between 300 and 500 nm. When the LCP is in the presence of amyloid-like fibrils, the fluorescence intensity increases significantly, doubling in the case of PTAA, and is slightly red-shifted. Often the excitation maximum is also

dx.doi.org/10.1021/jp305311z | J. Phys. Chem. B XXXX, XXX, XXX–XXX

red-shifted. When PTAA was tested with the His.Gln peptide solution, the change in fluorescence showed definitive signs of amyloid fibril formation (Figure 6). This was even more

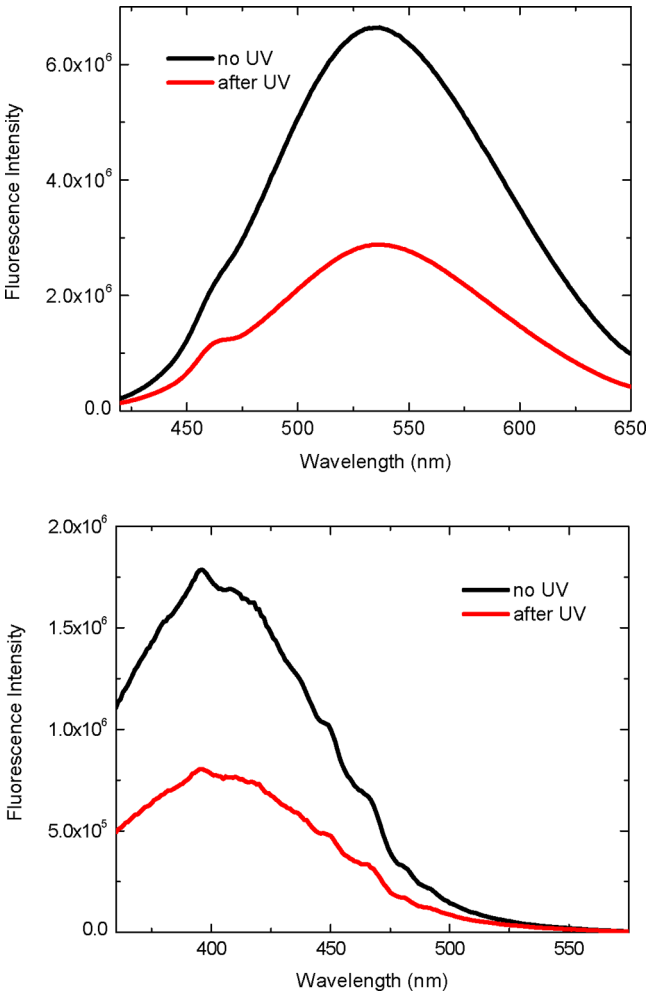

Figure 6. PTAA fluorescence. Fluorescence spectra of PTAA in solution with the His.Gln peptide before UV illumination (black), when light scattering measurements are high, and after UV illumination (red), when scattering measurements have reached the minimum intensity. Top: Emission spectra (excitation at 400 nm). Bottom: Excitation spectra (emission at 600 nm).

apparent when comparing the fluorescence emission spectra between the peptide solution before and after UV light exposure. Before exposure, when the level of peptide aggregation was high, the fluorescence intensity was greater than double that following photoinduced disassociation. Apart from the absence of blue shift in the excitation spectrum, the spectra appear consistent with those measured for PTAA in the presence and absence of Aβ peptide aggregation, as investigated previously.[55]

Transmission Electron Microscopy. To determine the morphology of the peptide assemblies, we produced a number of TEM micrographs of the samples taken after the initial aggregation, as well as following photoinduced disassociation and reaggregation. Initially aggregated His.Gln peptides clearly show the presence of fibrils with an average length of 400 nm, and 6−8 nm thickness (Figure 7a). The peptide solution was then exposed to UV light for 2 h and the scattering monitored. Samples were taken once the scattering intensity reached a

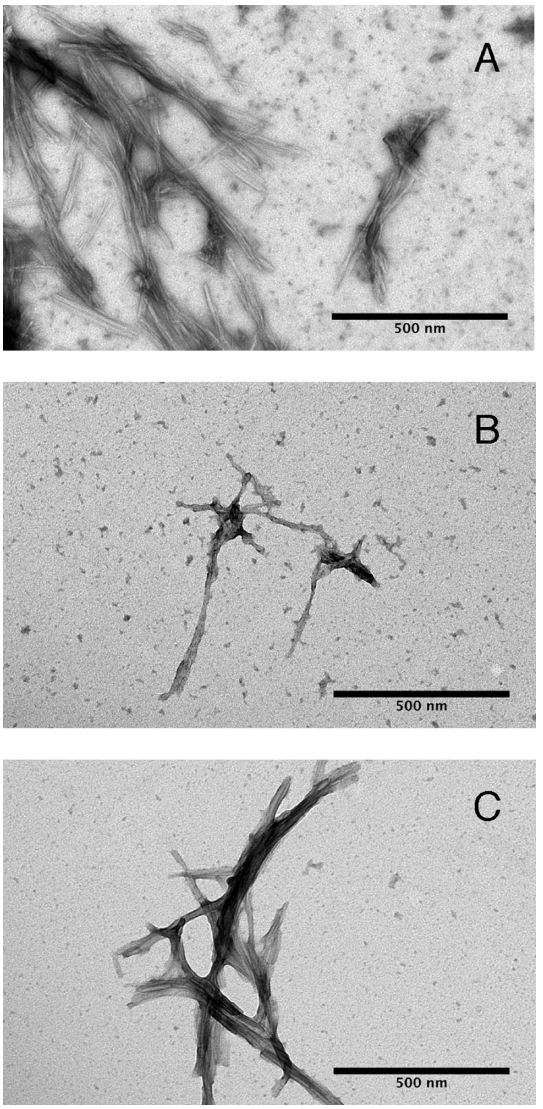

Figure 7. Transmission electron microscopy. (a) TEM image of amyloid-like fibrils formed by the His.Gln peptide at pH 7 with the photolinker in the trans conformation. (b) The same peptide at pH 7 after constant UV illumination forcing the photolinker into the cis conformation and fibrils to disassociate. The cis fibrils look shorter and more fragile than their trans counterparts. (c) The same peptide after illumination has been removed, and the photolinker has returned to the trans state, allowing reaggregation of the peptide.

stable minimum value. Subsequently, in the absence of UV light, aggregation was allowed to proceed and samples were taken when the light-scattering intensity had reached a maximum value, corresponding to the maximum amount of aggregated peptides. Both sets of samples were then used to produce TEM micrographs. In the samples taken after disassociation, it was difficult to find regions within the TEM grid that had aggregation and all visible aggregates were made of clumps of residual, not entirely fibrillar morphologies (Figure 7b). The samples taken after reaggregation contain fibrils indistinguishable from those observed following the initial aggregation step (Figure 7c).

V. DISCUSSION AND CONCLUSIONS

In this work, we designed and experimentally tested a minimal peptide that, cross-linked with an azobenzene group, self-

dx.doi.org/10.1021/jp305311z | J. Phys. Chem. B XXXX, XXX, XXX−XXX

associates into amyloid fibrils and dissociates from them in a photocontrollable manner. The peptide is comprised of only six residues and has a β-aggregation prone and a soluble conformation that are directed by the trans and cis conformation of the cross-linker. To maximize the effects of the photoisomerization, our design was driven by the search for the most β-aggregation prone mutant in the trans state, which at the same time has the highest possible solubility when in the cis state. Because of the minimal length of the peptide, it was only necessary to systematically screen the three central residues, flanked by the cross-linked cysteines. This allowed us to use equilibrium aggregation simulations of peptide trimers in implicit solvent to determine the aggregation properties of each of the possible sequences.

We then used the four most promising sequences to start implicit solvent aggregation simulations of octamers, from which we chose the final sequence, Ac-Cys-His-Gly-Gln-Cys-Lys-NH_2. The stability of ordered octamers, spontaneously formed by this sequence, were further validated in explicit solvent simulations. Finally, the cross-linked peptide was synthesized and tested by performing aggregation experiments monitored by light-scattering, fluorescence, and TEM. We conducted a reversible aggregation experiment where the sample was intermittently illuminated by UV-light, which switched the photolinker into the cis state, inducing dissociation, and then allowed to associate when the illumination was removed. Strikingly, the designed reversible photocontrolled fibrillation was confirmed by the light-scattering measurements and TEM micrographs. Moreover, the fluorescence assays corroborated the hypothesis of amyloid aggregation.

Molecular dynamics simulations of the octamer, both in implicit and explicit solvent, provided insights into the structural properties and dynamics of the amyloid formation process. The ordered oligomers formed when the cross-linker is in the trans state are organized into a double four-stranded parallel β-sheet, and the side chains are arranged to optimally interact with the solvent. In detail, the hydrophobic azobenzene moieties are buried inside the oligomer and stabilize the interface of the two β-sheets, and the peptides' polar side chains are pointing to the solvent. This "hydrophobic-in" and "polar-out" arrangement of the side chains is similar to those found in amyloid fibril models obtained from solid state NMR data.[58−60] The assembly is stabilized by a variety of intermolecular interactions. In addition to the peptide backbone hydrogen bonds typically present in amyloid aggregates, we also observed ordered benzene stacking in the hydrophobic core, and hydrogen bonds between the amide groups belonging to the cross-linkers. The oligomer explores different arrangements of benzene packing, agreeing with observation that the amyloid assemblies are dynamic and polymorphic.[8,61] It is worth noting that the cross-linker moiety, consisting of amide and benzene groups, mimics the functional groups of Asn/Gln and Phe/Tyr side chains, respectively, which are known to promote and stabilize amyloid structures as revealed by amyloid microcrystals[62,63] and kinetic measurements.[64−66] The selection of polar His and Gln residues at positions X_2 and X_4 derives from the maximization of the amphipathic moment of the sequence, which was indirectly imposed by the bias of the filtering process toward sequences that formed ordered and soluble structures at the same time. As mentioned above, glutamine and asparagine are common amino acids in all amyloid sequences. Less clear is the role of histidine, which was persistently highly ranked at position X_2. The pH dependence of aggregation detected in the experiment might be interpreted as an effect of the protonation state of the histidine. Below pH 6, the peptides do not aggregate, due to the electrostatic repulsion exerted by protonated histidine. Therefore, this amino acid must have an important stabilization role in the aggregation. Interestingly, histidine appears close to glutamine and asparagine in aggregation hotspots belonging to β-amyloid peptide H_{13}HQKLVFF$_{20}$ and in the islet amyloid polypeptide H_{18}SSNNFGAIL$_{27}$. In both cases, protonated histidines or histidine mutations impaired protofilament self-assembly for β-amyloid peptide[67] and noticeably slowed down aggregation kinetics of islet amyloid polypeptide.[68]

Ordered aggregation spontaneously nucleates in the simulations as a two-step process within a disordered micellar oligomer. Initially, a single β-sheet assembles and successively induces the formation of the second β-sheet. This scenario is consistent with the nucleated conformational conversion (NCC) mechanism,[69] where monomers initially assemble into amorphous oligomers, and then convert into ordered oligomers that are able to nucleate the fibril formation. On-pathway disordered oligomers have been observed for a number of polypeptide sequences, including Sup35 prion,[69] Aβ peptide,[70] and SH3 domain,[71] and have been very well characterized by simplified peptide simulations.[34,72−74] Due to the amphipathic nature of the cross-linked His.Gln peptide, oligomers formed in the cis state have a micellar structure very similar to the early amorphous oligomers formed in the trans state. We can speculate that during UV illumination the fibrils quickly dissociate into micelles composed of cis monomers. When illumination is removed, nucleation occurs in the preexisting oligomers which act as seeds, explaining the more reproducible reaggregation kinetics with respect to the initial aggregation, when the oligomers were not present. It is worth noting that the aggregation kinetics of the simulations are apparently orders of magnitude faster than the ones observed in the experiments. This is due to the much lower friction coefficient of the implicit solvent with respect to real solvent, which is about 100 times more viscous, and also due to the higher peptide concentration of the simulated system (5.3 mM) with respect to the experimental sample (0.3 mM). Furthermore, as revealed by the TEM micrographs of the disaggregated samples, the light scattering experiment is not sensitive enough to detect small oligomers, which most likely form much earlier than amyloid fibrils.

The highly ordered octamer conformation suggests a possible structural model for the fibrils observed in the TEM micrographs, where a single protofilament is obtained by replicating the oligomer along its β-sheet axis. However, the thickness of the fibril observed in TEM micrographs (about 60−80 Å) is incompatible with the 15−25 Å inter-β-sheet thickness of the oligomer formed in silico. We can speculate that several identical protofilaments are bundled together and stabilized by side chain steric zipper interaction through the protofilament hydrophilic surface, as observed in amyloid microcrystals.[62] It is also important to note that individual oligomer strands of the order of 20 Å thick are difficult to detect with TEM using the negative staining techniques employed in these measurements.

The peptide presented here may have several applications. First, as described in this work, the photoswitchable peptide can be used to control the amyloid aggregation process. Second, the cross-linked peptide can be embedded in a larger sequence and

dx.doi.org/10.1021/jp305311z | J. Phys. Chem. B XXXX, XXX, XXX−XXX

can act as a controllable amyloid hot-spot. Finally, by varying the intensity of UV illumination, it is possible to change the equilibrium population ratio between cis and trans states and effectively control the population difference between the β-aggregation prone and the soluble conformations of the peptides in the sample, modulating the pathways of the amyloid aggregation, as previously illustrated by a coarse grained model of an amphipathic amyloid peptide.[75]

■ ASSOCIATED CONTENT

Supporting Information

Figures S1 and S2: Time series of the number of inter- and intramolecular backbone hydrogen bonds of the octamer aggregation simulations in the cis and trans conformations. Figure S3: Histogram of the radius of gyration for the 26 aggregation simulations of the trimer in cis configurations. Table S1: Rank of the $X_2.X_4$ trimer sequences simulated with SASA. Tables S2 and S3: Ranks of the $X_2.X_4$ trimer sequences simulated with FACTS. Figure S4: Aggregation forming on the cuvette surfaces and in the solution. This material is available free of charge via the Internet at http://pubs.acs.org.

■ AUTHOR INFORMATION

Corresponding Author

*Phone: +41 44 635 55 21. Fax: +41 44 635 68 62. E-mail: phamm@pci.uzh.ch (P.H.), caflisch@bioc.uzh.ch (A.C.), pellarin@salilab.org (R.P.).

Notes

The authors declare no competing financial interest.

■ ACKNOWLEDGMENTS

The simulations were performed on the Schrödinger cluster of the University of Zurich, and we gratefully acknowledge the support of C. Bolliger and A. Godknecht. We thank Prof. A. Aguzzi and Dr. S. Hornemann for providing LCP samples and helpful discussions. TEM imaging was performed with equipment maintained by the Center for Microscopy and Image Analysis, University of Zurich, who also provided much support and assistance with the image analysis. This work was supported by a Swiss National Science Foundation grant and NCCR Neuro grant to A.C. and an Advanced Investigator ERC grant (Dynallo) to P.H.

■ REFERENCES

(1) Merlini, G.; Bellotti, V. *N. Engl. J. Med.* **2003**, *349*, 583−596.
(2) Sunde, M.; Blake, C. *Adv. Protein Chem.* **1997**, *50*, 123−159.
(3) Makin, O. S.; Atkins, E.; Sikorski, P.; Johansson, J.; Serpell, L. C. *Proc. Natl. Acad. Sci. U.S.A.* **2005**, *102*, 315−320.
(4) Chiti, F.; Dobson, C. M. *Annu. Rev. Biochem.* **2006**, *75*, 333−366.
(5) Kelly, J. W. *Curr. Opin. Struct. Biol.* **1998**, *8*, 101−106.
(6) Fändrich, M. *J. Mol. Biol.* [Online early access]. DOI: 10.1016/j.jmb.2012.01.006. Published Online Jan 12, **2012**.
(7) Lomakin, A.; Chung, D. S.; Benedek, G. B.; Kirschner, D. A.; Teplow, D. B. *Proc. Natl. Acad. Sci. U.S.A.* **1996**, *93*, 1125−1129.
(8) Kodali, R.; Wetzel, R. *Curr. Opin. Struct. Biol.* **2007**, *17*, 48−57.
(9) Shim, S.-H.; Gupta, R.; Ling, Y. L.; Strasfeld, D. B.; Raleigh, D. P.; Zanni, M. T. *Proc. Natl. Acad. Sci. U.S.A.* **2009**, *106*, 6614−6619.
(10) Esler, W. P.; Stimson, E. R.; Jennings, J. M.; Vinters, H. V.; Ghilardi, J. R.; Lee, J. P.; Mantyh, P. W.; Maggio, J. E. *Biochemistry* **2000**, *39*, 6288−6295.
(11) Vitalis, A.; Wang, X.; Pappu, R. V. *Biophys. J.* **2007**, *93*, 1923−1937.
(12) Vitalis, A.; Lyle, N.; Pappu, R. V. *Biophys. J.* **2009**, *97*, 303−311.
(13) Gsponer, J.; Haberthür, U.; Caflisch, A. *Proc. Natl. Acad. Sci. U.S.A.* **2003**, *100*, 5154−5159.
(14) Hwang, W.; Zhang, S.; Kamm, R. D.; Karplus, M. *Proc. Natl. Acad. Sci. U.S.A.* **2004**, *101*, 12916−12921.
(15) de la Paz, M. L.; de Mori, G. M. S.; Serrano, L.; Colombo, G. *J. Mol. Biol.* **2005**, *349*, 583−596.
(16) Cecchini, M.; Curcio, R.; Pappalardo, M.; Melki, R.; Caflisch, A. *J. Mol. Biol.* **2006**, *357*, 1306−1321.
(17) Strodel, B.; Whittleston, C. S.; Wales, D. J. *J. Am. Chem. Soc.* **2007**, *129*, 16005−16014.
(18) Simone, A. D.; Esposito, L.; Pedone, C.; Vitagliano, L. *Biophys. J.* **2008**, *95*, 1965−1973.
(19) Bellesia, G.; Shea, J.-E. *Biophys. J.* **2009**, *96*, 875−886.
(20) Ma, B.; Nussinov, R. *Proc. Natl. Acad. Sci. U.S.A.* **2002**, *99*, 14126−14131.
(21) Buchete, N.-V.; Tycko, R.; Hummer, G. *J. Mol. Biol.* **2005**, *353*, 804−821.
(22) Wu, C.; Bowers, M. T.; Shea, J.-E. *PLoS Comput. Biol.* **2010**, *6*, e1000693.
(23) Berryman, J. T.; Radford, S. E.; Harris, S. A. *Biophys. J* **2009**, *97*, 1−11.
(24) Krone, M. G.; Hua, L.; Soto, P.; Zhou, R.; Berne, B. J.; Shea, J.-E. *J. Am. Chem. Soc.* **2008**, *130*, 11066−11072.
(25) Santini, S.; Mousseau, N.; Derreumaux, P. *J. Am. Chem. Soc.* **2004**, *126*, 11509−11516.
(26) Reddy, G.; Straub, J. E.; Thirumalai, D. *Proc. Natl. Acad. Sci. U.S.A.* **2009**, *106*, 11948−11953.
(27) Strodel, B.; Lee, J. W. L.; Whittleston, C. S.; Wales, D. J. *J. Am. Chem. Soc.* **2010**, *132*, 13300−13312.
(28) Vitagliano, L.; Stanzione, F.; De Simone, A.; Esposito, L. *Biopolymers* **2009**, *91*, 1161−1171.
(29) Nasica-Labouze, J.; Meli, M.; Derreumaux, P.; Colombo, G.; Mousseau, N. *PLoS Comput. Biol.* **2011**, *7*, e1002051.
(30) Convertino, M.; Pellarin, R.; Catto, M.; Carotti, A.; Caflisch, A. *Protein Sci.* **2009**, *18*, 792−800.
(31) Scherzer-Attali, R.; Pellarin, R.; Convertino, M.; Frydman-Marom, A.; Egoz-Matia, N.; Peled, S.; Levy-Sakin, M.; Shalev, D. E.; Caflisch, A.; Gazit, E.; Segal, D. *PLoS One* **2010**, *5*, e11101.
(32) Frydman-Marom, A.; Convertino, M.; Pellarin, R.; Lampel, A.; Shaltiel-Karyo, R.; Segal, D.; Caflisch, A.; Shalev, D. E.; Gazit, E. *ACS Chem. Biol.* **2011**, *6*, 1265−1276.
(33) Chebaro, Y.; Derreumaux, P. *Proteins* **2009**, *75*, 442−452.
(34) Nguyen, H. D.; Hall, C. K. *Proc. Natl. Acad. Sci. U.S.A.* **2004**, *101*, 16180−16185.
(35) Nguyen, P. H.; Li, M. S.; Stock, G.; Straub, J. E.; Thirumalai, D. *Proc. Natl. Acad. Sci. U.S.A.* **2007**, *104*, 111−116.
(36) LeVine, H., III. *Arch. Biochem. Biophys.* **1997**, *342*, 306−316.
(37) Soto, C.; Castaño, E. M.; Kumar, R. A.; Beavis, R. C.; Frangione, B. *Neurosci. Lett.* **1995**, *200*, 105−108.
(38) Camus, M.-S.; Dos Santos, S.; Chandravarkar, A.; Mandal, B.; Schmid, A. W.; Tuchscherer, G.; Mutter, M.; Lashuel, H. A. *ChemBioChem* **2008**, *9*, 2104−2112.
(39) Taniguchi, A.; Skwarczynski, M.; Sohma, Y.; Okada, T.; Ikeda, K.; Prakash, H.; Mukai, H.; Hayashi, Y.; Kimura, T.; Hirota, S.; Matsuzaki, K.; Kiso, Y. *ChemBioChem* **2008**, *9*, 3055−3065.
(40) Hamill, A. C.; Wang, S.-C.; Lee, C. T., Jr. *Biochemistry* **2007**, *46*, 7694−7705.
(41) Hamill, A.; Lee, C. *J. Phys. Chem. B* **2009**, *113*, 6164.
(42) Matsuzawa, Y.; Ueki, K.; Yoshida, M.; Tamaoki, N.; Nakamura, T.; Sakai, H.; Abe, M. *Adv. Funct. Mater.* **2007**, *17*, 1507−1514.
(43) Vollmer, M.; Clark, T.; Steinem, C.; Ghadiri, M. *Angew. Chem., Int. Ed.* **1999**, *38*, 1598−1601.
(44) Aemissegger, A.; Krautler, V.; van Gunsteren, W. F.; Hilvert, D. *J. Am. Chem. Soc.* **2005**, *127*, 2929−2936.
(45) Deeg, A.; Schrader, T.; Kempter, S.; Pfizer, J.; Moroder, L.; Zinth, W. *ChemPhysChem* **2011**, *12*, 559−562.
(46) Brooks, B. R.; Brooks, C. L., III; Mackerell, A. D.; Nilsson, L.; Petrella, R. J.; Roux, B.; Won, Y.; Archontis, G.; Bartels, C.; Boresch, S.; et al. *J. Comput. Chem.* **2009**, *30*, 1545−1614.

(47) Ferrara, P.; Apostolakis, J.; Caflisch, A. *Proteins* **2002**, *46*, 24−33.
(48) Haberthür, U.; Caflisch, A. *J. Comput. Chem.* **2008**, *29*, 701−715.
(49) Ryckaert, J.-P.; Ciccotti, G.; Berendsen, H. J. C. *J. Comput. Phys.* **1977**, *23*, 327−341.
(50) Pasini, P.; Zannoni, C.; Žumer, S. *Computer Simulations of Liquid Crystals and Polymers*; Kluwer Academic Publishers: Dordrecht, the Netherlands, 2005.
(51) Allen, M. P.; Tildesley, D. J. *Computer Simulation of Liquids*; Oxford University Press: New York, 1989.
(52) Cecchini, M.; Rao, F.; Seeber, M.; Caflisch, A. *J. Chem. Phys.* **2004**, *121*, 10748−10756.
(53) Paoli, B.; Seeber, M.; Backus, E. H. G.; Ihalainen, J. A.; Hamm, P.; Caflisch, A. *J. Phys. Chem. B* **2009**, *113*, 4435−4442.
(54) Kumita, J. R.; Smart, O. S.; Woolley, G. A. *Proc. Natl. Acad. Sci. U.S.A.* **2000**, *97*, 3803−3808.
(55) Nilsson, K. P. R.; Åslund, A.; Berg, I.; Nyström, S.; Konradsson, P.; Herland, A.; Inganäs, O.; Stabo-Eeg, F.; Lindgren, M.; Westermark, G. T.; et al. *ACS Chem. Biol.* **2007**, *2*, 553−560.
(56) Nilsson, M. R. *Methods* **2004**, *34*, 151−160.
(57) Nilsson, K. P. R.; Herland, A.; Hammarström, P.; Inganäs, O. *Biochemistry* **2005**, *44*, 3718−3724.
(58) Wasmer, C.; Soragni, A.; Sabate, R.; Lange, A.; Riek, R.; Meier, B. H. *Angew. Chem., Int. Ed. Engl.* **2008**, *47*, 5839−5841.
(59) Petkova, A. T.; Ishii, Y.; Balbach, J. J.; Antzutkin, O. N.; Leapman, R. D.; Delaglio, F.; Tycko, R. *Proc. Natl. Acad. Sci. U.S.A.* **2002**, *99*, 16742−16747.
(60) Lührs, T.; Ritter, C.; Adrian, M.; Riek-Loher, D.; Bohrmann, B.; Döbeli, H.; Schubert, D.; Riek, R. *Proc. Natl. Acad. Sci. U.S.A.* **2005**, *102*, 17342−17347.
(61) Carulla, N.; Caddy, G. L.; Hall, D. R.; Zurdo, J.; Gairi, M.; Feliz, M.; Giralt, E.; Robinson, C. V.; Dobson, C. M. *Nature* **2005**, *436*, 554−558.
(62) Nelson, R.; Sawaya, M. R.; Balbirnie, M.; Madsen, A. O.; Riekel, C.; Grothe, R.; Eisenberg, D. *Nature* **2005**, *435*, 773−778.
(63) Sawaya, M. R.; Sambashivan, S.; Nelson, R.; Ivanova, M. I.; Sievers, S. A.; Apostol, M. I.; Thompson, M. J.; Balbirnie, M.; Wiltzius, J. J. W.; McFarlane, H. T.; et al. *Nature* **2007**, *447*, 453−457.
(64) Gazit, E. *FASEB J* **2002**, *16*, 77−83.
(65) Azriel, R.; Gazit, E. *J. Biol. Chem.* **2001**, *276*, 34156−34161.
(66) Tracz, S. M.; Abedini, A.; Driscoll, M.; Raleigh, D. P. *Biochemistry* **2004**, *43*, 15901−15908.
(67) Fraser, P. E.; McLachlan, D. R.; Surewicz, W. K.; Mizzen, C. A.; Snow, A. D.; Nguyen, J. T.; Kirschner, D. A. *J. Mol. Biol.* **1994**, *244*, 64−73.
(68) Abedini, A.; Raleigh, D. P. *Biochemistry* **2005**, *44*, 16284−16291.
(69) Serio, T. R.; Cashikar, A. G.; Kowal, A. S.; Sawicki, G. J.; Moslehi, J. J.; Serpell, L.; Arnsdorf, M. F.; Lindquist, S. L. *Science* **2000**, *289*, 1317−1321.
(70) Yong, W.; Lomakin, A.; Kirkitadze, M. D.; Teplow, D. B.; Chen, S.-H.; Benedek, G. B. *Proc. Natl. Acad. Sci. U.S.A.* **2002**, *99*, 150−154.
(71) Carulla, N.; Zhou, M.; Arimon, M.; Gairí, M.; Giralt, E.; Robinson, C. V.; Dobson, C. M. *Proc. Natl. Acad. Sci. U.S.A.* **2009**, *106*, 7828−7833.
(72) Pellarin, R.; Caflisch, A. *J. Mol. Biol.* **2006**, *360*, 882−892.
(73) Auer, S.; Meersman, F.; Dobson, C. M.; Vendruscolo, M. *PLoS Comput. Biol.* **2008**, *4*, e1000222.
(74) Bellesia, G.; Shea, J.-E. *J. Chem. Phys.* **2009**, *131*, 111102.
(75) Pellarin, R.; Guarnera, E.; Caflisch, A. *J. Mol. Biol.* **2007**, *374*, 917−924.
(76) Jorgensen, W. L.; Chandrasekhar, J.; Madura, J. D.; Impey, R. W.; Klein, M. L. *J. Chem. Phys.* **1983**, *79*, 926.